Effects of scars on icosahedral crystalline shell stability under external pressure

Duanduan Wan, Mark J. Bowick, and Rastko Sknepnek

Phys. Rev. E **91**, 033205 — Published 19 March 2015

DOI: 10.1103/PhysRevE.91.033205

Effects of scars on icosahedral crystalline shell stability under external pressure

Duanduan Wan,[1] Mark J. Bowick,[1,2,*] and Rastko Sknepnek[3]

[1] *Department of Physics, Syracuse University, Syracuse NY 13244, USA*
[2] *Syracuse Biomaterials Institute, Syracuse University, Syracuse NY 13244, USA*
[3] *Division of Physics and Division of Computational Biology, University of Dundee, Dundee DD1 4HN, UK*

We study how the stability of spherical crystalline shells under external pressure is influenced by the defect structure. In particular, we compare stability for shells with a minimal set of topologically-required defects to shells with extended defect arrays (grain boundary "scars" with non-vanishing net disclination charge). We perform both Monte Carlo and conjugate gradient simulations to compare how shells with and without scars deform quasi-statically under external hydrostatic pressure. We find that the critical pressure at which shells collapse is lowered for scarred configurations that break icosahedral symmetry and raised for scars that preserve icosahedral symmetry. The particular shapes which arise from breaking of an initial icosahedrally-symmetric shell depend on the Föppl-von Kármán number.

PACS numbers: 46.32.+x, 46.70.De, 61.72.-y, 11.30.Qc

I. INTRODUCTION

Thin elastic shells with spherical topology are ubiquitous in nature. Examples span a vast range of length scales: viral capsids [1] and nanocages [2] at the nano-scale, pollen grains [3] at the micro-scale, ping-pong balls [4] and stadium domes in the centimeter to decameter range and the Earth's crust on the scale of the entire planet. Despite the breadth of scales, all such shells may be considered thin, as measured by their thickness h in terms of their linear size R (i.e., $h/R \ll 1$). As for thin plates, the mechanics of shells can be described in a continuum approach that expands the elastic energy in powers of the thickness [5]. The resulting theory is non-linear even in the limit of small strains, as bending deformations ($O(h^3)$) [6] play a significant role. In contrast to plates, however, any deformation of a shell couples stretching and bending [7, 8], with remarkable consequences for the effect of thermal fluctuations on the material properties of the shell [9]. This is a consequence of the so-called *geometric rigidity* of the sphere [8] - any deformation of the sphere is accompanied by a change of the local Gaussian curvature. The Gaussian curvature and the metric of a surface are intimately related (as recognized over two centuries ago by Gauss [10]), and any change of Gaussian curvature will lead to changes in the metric, resulting in stretching or compression.

The situation is particularly striking if the shell is small enough that its crystalline structure plays a role. It is well known that perfect crystalline order is incompatible with spherical topology. In other words, it is not possible to cover a two-sphere with identical particles such that each one has exactly six equidistant nearest neighbors. Instead one needs to introduce topological defects - special points that have coordination number different than six. More precisely, topology requires that $\sum_i (6 - c_i) = 6\chi = 12$ for any triangulation of a two-sphere, where c_i is the coordination number of vertex i and $\chi = 2$ is the Euler characteristic of the two-sphere. The quantity $q_i = 6 - c_i$ is called the disclination charge and measures the departure from the perfect triangular order of the plane. Provided we restrict ourselves to the energetically preferred charge $q = \pm 1$ disclinations, the topological constraint becomes $N_{+1} - N_{-1} = 12$ and we see that a spherical crystal must have at least twelve $+1$ disclinations. These disclinations may also be viewed as singular concentrations of Gaussian curvature and in essence screen it [11], thus lowering the elastic stress. With the defects being inherently discrete this screening cannot be perfect and the crystal will retain a certain level of residual stress even in the ground state. This has profound consequences for the mechanical behavior of the shell.

Limited to the minimal set of defects, the twelve disclinations repel each other, much like electric charges in two dimensions, and arrange themselves to minimize the total energy. For an icosadeltahedral triangulation, the defects are located at the twelve vertices of an inscribed icosahedron and all possible crystal lattices can be constructed following the prescription of Caspar and Klug [12]. In this approach each lattice is labelled by a pair of integers, (p, q) that together form the T-number, $T = p^2 + pq + q^2$, with the total number of lattice sites being given by $N = 10T + 2$. For a sufficiently large number of particles, however, and provided the defect core energy is not very high, the ground state of a spherical crystal will have finite-length grain boundary *scars* of tightly bound $5 - 7$ pairs radiating from the original $+1$ disclinations [13, 14]. This phenomenon was also observed earlier [15] in a study of the Thomson problem [16] of determining the ground state of classical electrons interacting with a repulsive Coulomb potential on the surface of a two-sphere. Scars have been observed experimentally in colloidal suspensions on spherical droplets - colloidosomes [17, 18] - and in bubble rafts on a paraboloidal surface [19].

* Correspondence should be sent to:bowick@phy.syr.edu

If allowed to deform the shell can relieve some of the residual stress caused by the disclination defects by buckling. This was first discussed by Seung and Nelson [20] in the context of a single planar disclination. They showed that for a sufficiently large disclination radius R it is energetically favorable to buckle into a cone with the apex at the disclination. The system reduces its stretching energy at the expense of gaining some bending energy. The transition occurs as the ratio of the energy scales that control the relative strength of bending vs. stretching, the so-called Föppl-von Kármán number $\gamma = YR^2/\kappa \propto \left(\frac{R}{h}\right)^2$, exceeds a critical value of ≈ 154 ($Y \propto h$ is the two-dimensional (2D) Young's modulus and $\kappa \propto h^3$ is the bending rigidity). On a sphere, the same mechanism drives a simultaneous buckling of all 12 disclinations leading to a transition from a sphere to an icosahedron [21]. The transition is rounded compared to the flat case, and shifted to slightly higher values of γ. Buckling into an icosahedron is quite robust and is not qualitatively affected by imposing volume constants [22] or by the presence of scars [23].

The stability of thin crystalline shells under external pressure is at present only partly understood. Physical examples include suspensions of viruses in solution [22, 24, 25], drug-delivery microcapsules in a flow [26] and polyelectrolyte capsules in osmotic deswelling experiments [27]. Buckling of spherical shells with soft spots under external pressure has been considered in Ref. [28]. The elastic theory of shells predicts the mechanical response of an ideal spherical shell under external pressure [6]. On microscopic scales crystalline order and defects may affect the stability of crystalline shells under external pressure.

The paper is organized as follows. In Section II we present a discrete model for a shell under pressure. In Section III we analyze this model using both Monte Carlo and conjugate gradient simulations and discuss how the critical pressure at which the shell collapses is related to the symmetry of the scars. In Section IV we use spherical harmonic expansion to characterize symmetries of collapsing shells. Finally, in Section V we summarize the main results and reflect on the possible extensions of this work.

II. MODEL

In thin plate elasticity theory, a deformation is represented by an in-plane displacement vector field $\mathbf{u}(\mathbf{r}) = (u_1, u_2)$ and an out-of-plane displacement ("deflection") field $f(\mathbf{r})$, which map the point $(x_1, x_2, 0)$ in the reference state to $(x_1 + u_1, x_2 + u_2, f)$. The elastic energy of an isotropic thin plate is the sum of a stretching and a bending energy [5, 7], $F_{el} = F_s + F_b$. In the regime of linear response, i.e., for small strains, the stretching energy is

$$F_s = \frac{1}{2}\int dS \left(2\mu u_{ij}^2 + \lambda u_{kk}^2\right), \tag{1}$$

where

$$u_{ij} = \frac{1}{2}\left(\partial_i u_j + \partial_j u_i + \partial_i u_k \partial_j u_k + \partial_i f \partial_j f\right) \tag{2}$$

is the exact form of the strain tensor (indices run over 1 and 2) and the displacement fields are evaluated along the center surface. For small displacement gradients, the terms quadratic in u_k could be neglected but the term quadratic in f needs to be retained as there is no term of lower order in f. μ and λ are the 2D Lamé coefficients and the integral is over the area of the reference state. The 2D Young's modulus $Y = Eh$ (E being the full three-dimensional Young's modulus) and Poisson ratio ν can be expressed in terms of the 2D Lamé coefficients as [20]

$$Y = \frac{4\mu(\mu+\lambda)}{2\mu+\lambda}, \qquad \nu = \frac{\lambda}{2\mu+\lambda}. \tag{3}$$

The bending energy is

$$F_b = \frac{1}{2}\kappa \int dS \left(\left(\nabla^2 f\right)^2 - 2(1-\nu)\det\left(\partial_i\partial_j f\right)\right), \tag{4}$$

where $\kappa = Eh^3/12\left(1-\nu^2\right)$ [5] is the bending rigidity. In terms of f, twice the mean curvature H and Gaussian curvature K ($H = 1/R_1 + 1/R_2$, $K = 1/R_1R_2$, with R_1 and R_2 being the principal radii of curvature, respectively) can be written as [29]

$$H = \nabla\cdot\left(\frac{\nabla f}{\sqrt{1+|\nabla f|^2}}\right), \quad K = \frac{\det\left(\partial_i\partial_j f\right)}{\left(1+|\nabla f|^2\right)^2}. \tag{5}$$

For small $|\nabla f|$,

$$H \approx \nabla^2 f, \quad K \approx \det\left(\partial_i\partial_j f\right), \tag{6}$$

and the bending energy F_b can be rewritten in the form of the Helfrich bending energy as

$$F_b \approx \int dS \left(\frac{1}{2}\kappa H^2 + \kappa_G K\right), \tag{7}$$

where $\kappa_G = -Eh^3/12(1+\nu)$ is the Gaussian rigidity.

Within a discretized model where the flat plate is represented as a perfect triangular lattice, upon deformation, the stretching energy is given as [20, 21, 30]

$$F_s = \frac{\varepsilon}{2}\sum_{\langle ij\rangle}\left(|\mathbf{r}_i - \mathbf{r}_j| - a\right)^2, \tag{8}$$

and the bending energy is given as

$$F_b = \frac{\tilde{\kappa}}{2}\sum_{\langle IJ\rangle}\left(\hat{\mathbf{n}}_I - \hat{\mathbf{n}}_J\right)^2, \tag{9}$$

where $\langle ij \rangle$ denote pairs of nearest neighbor vertices, with positions $\mathbf{r}_i$ in the embedding three-dimensional space. a is the equilibrium distance (the spacing in the flat state) and ε is the elastic spring constant. $\tilde{\kappa}$ is the discrete bending modulus and $\langle IJ \rangle$ denote pairs of nearest neighbor triangular plaquette, with unit normals $\hat{\mathbf{n}}_I$. In the continumm limit of a sufficiently large number of triangular plaquettes, it has been shown that in infinitesimal elasticity regime $Y = 2\varepsilon/\sqrt{3}$, $\nu = 1/3$ [20, 30] and for isometric immersions, Eq. (9) becomes [30]

$$F_b = \frac{\tilde{\kappa}}{4\sqrt{3}} \int dS \left(3H^2 - 8K\right), \tag{10}$$

which has the form of Eq. (7), with $\kappa = \sqrt{3}\tilde{\kappa}/2$ and $\kappa_G = -4\kappa/3$. Eq. (10) provides a good approximation to the energy in bending-dominated deformation regime (an almost isometric immersion, a perfect isometric immersion implies pure bending and $K \equiv 0$) and general surfaces can be triangulated with an almost isometric immersion by a partition of the surface into regions of area on a mesoscopic scale and allowing for defects in the reference lattice along the boundary of these regions [30].

In the numerical simulation we consider a discrete triangulated shell with the elastic energy being a sum of the stretching and bending energies given in Eqs. (8) and (9). Shells without scars are constructed using the Caspar-Klug procedure (i.e., in terms of (p, q) pairs), with the equilibrium distance a being chosen as the mean value of all edge lengths over the entire triangulation (due to spherical topology not all edges can have equal length) and radii rescaled such that $a = 1$. We choose a as the length unit in this work. At the same time, we choose $\tilde{\kappa} = 1$ as the energy unit, so the pressure is in units of $\tilde{\kappa}/a^3$ and the units of other parameters follow the same rule. Shells with scars have the same total number of vertices and initial radii as shells without scars, with the connectivity matrix taken from the Thomson problem database [31]. We use two methods: Monte Carlo and conjugate gradient. In the Monte Carlo approach, to eliminate possible effects of thermal fluctuations, i.e., in the zero temperature limit, we set $k_B T = 10^{-11}$. The maximal step size is set to 5×10^{-4} and the pressure is increased by 10^{-4} if the acceptance rate remains zero for ten consecutive sweeps. In the conjugate gradient method, the pressure is increased by 10^{-4} each time an equilibrated configuration is reached. During the simulation the connectivity of the triangular mesh is held fixed as the shell's shape changes. In other words, we assume that the defects are frozen, consistent with the much slower defect dynamics compared to shape relaxation [32]. Both methods seek to find local minima that are smooth deformations of the initial state. As the conjugate gradient method fails to produce unequilibrated configurations, e.g., those shown in Fig. 6, we analyze these configurations using the Monte Carlo method. We apply both methods to study the critical pressure and find that except for small deviations that we think are due to slight roughness in the energy landscape, the main results can be obtained using both methods. For consistency we shall only show the results of the Monte Carlo method.

III. NUMERICAL RESULTS

With the triangulation for shells without scars built following the (p, q) structure and the connectivity matrix for shells with scar defects being that of the lowest energy configuration found for the Thomson problem, we start by noting that, in the absence of external pressure, the equilibrated scarred shells have lower elastic energy compared to the equilibrated non-scarred shells for small values of ε. As ε increases, shells without scars may release some stress by buckling at the twelve disclinations [21] and find configurations with lower elastic energy than those formed by shells with scars.

As we do not focus on the global energy minimum state of shells in the absence of external pressure, as studied in Ref. [23] or its evolution as a function of external pressure, which would require simultaneous relaxation of both the topography and connectivity (i.e., allow for defect motion), we only study how the symmetry of the scar distribution in the initial configuration affects shell's tendency to succumb to pressure. We assume that the crystalline lattice on shells without scars always have icosahedral symmetry while shells with scars may break this symmetry. We therefore compare how shells without and with scars deform if the pressure is applied quasistatically. We present results of shells with $N_1 = 642$ ($(p, q) = (8, 0)$) and $N_2 = 1212$ ($(p, q) = (11, 0)$) as generic examples of cases where scars, respectively, break and preserve the icosahedral symmetry.

Fig. 1 shows some examples of equilibrated shells in the absence of external pressure. In the $N_1 = 642$ case, the scar-free lattice has an $(8, 0)$ structure, while the shells with scars have twelve five-seven-five scars of C_2 symmetry due to their mutual orientation. In the $N_2 = 1212$ case, shells without scars have an $(11, 0)$ structure while shells with scars have twelve identical star-like scars which preserve the icosahedral symmetry. For shells without scars the mean "asphericity" [21] (i.e., the deviation from a perfect spherical shape) departs significantly from zero when $\gamma \gtrsim 10^2$.

In the presence of an external hydrostatic pressure P, an additional term, PV, has to be added to the elastic energy functional, such that $F_{tot} = F_{el} + PV$. To quantify the deformation of shape, we first introduce a dimensionless parameter $\beta = (36\pi)^{\frac{1}{6}} V^{\frac{1}{3}}/A^{\frac{1}{2}}$, where V and A are volume and surface area, respectively. β provides a quantitative measure of the extent of convexity of the shell, with $\beta = 1$ for a sphere and $\beta \approx 0.969$ for an icosahedron. β decreases as the shell deflates under pressure. In our simulations, we set a lower limit $\beta_{min} = 0.6$ to avoid unphysical self-intersections when the system is

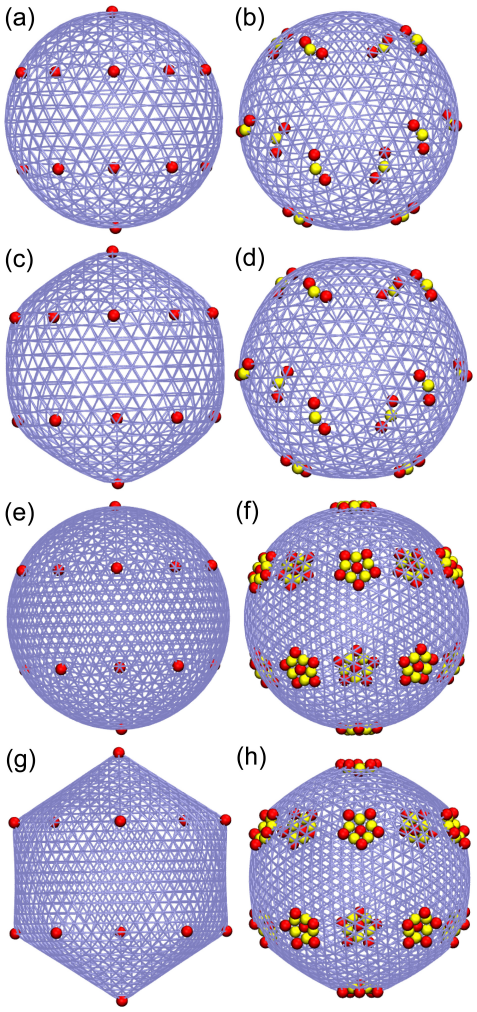

FIG. 1. (Color online) (a)-(d) Shells without scars have a $(p, q) = (8, 0)$ lattice structure (left) and shells with scars have twelve $5-7-5$ scars of C_2 symmetry (axis along the z direction) (right), with $\varepsilon = 1$ ($\gamma \approx 59$) (up) and $\varepsilon = 8$ ($\gamma \approx 474$) (down). (e)-(h) Shells without scars have a $(p, q) = (11, 0)$ structure (left) and shells with scars have twelve star-like scars of I symmetry (right), with $\varepsilon = 1$ ($\gamma \approx 112$) (up) and $\varepsilon = 64$ ($\gamma \approx 7149$) (down). The total number of vertices is $N_1 = 642$ and $N_2 = 1212$, respectively. Five-fold disclinations are shown in red (dark) and seven-fold in yellow (bright). Snapshots were generated using the Visual Molecular Dynamics (VMD) package [33] and rendered using the Tachyon ray tracer [34].

close to full collapse. We find that for small values of ε, shells collapse discontinuously to β_{min}, as shown in Fig. 2(a). The discontinuity defines a critical pressure P_c at which the shell can no longer retain its shape and collapses. For larger values of ε shells collapse in stages, as shown in Fig. 2(b). In this case we define P_c as the pressure at the first collapse. For even larger values of ε the collapse tends to become continuous and a definition of the critical pressure becomes more ambiguous. Here we only consider values of ε for which P_c can be unambiguously defined. In the $N_1 = 642$ ($(p, q) = (8, 0)$) case, shells without scars always have a higher value of P_c, as shown in Fig. 3(a). In contrast, shells with scars appear to always have a higher critical pressure in the $N_2 = 1212$ ($(p, q) = (11, 0)$) case, as shown in Fig. 3(b). In both cases, in the regime of small ε, where the mean "asphericity" does not depart significantly from zero in the absence of external pressure, the critical pressures are close to the buckling pressures $p \equiv 4\sqrt{\kappa Y}/R^2$ of an ideal spherical shell, as predicted by continuum elastic theory [6, 9].

IV. DISCUSSION

To gain a better understanding of the critical pressure, as an example we show in Fig. 4 the evolution of the system energy F_{tot} with $\varepsilon = 8$ along with the corresponding shell configurations before collapse. The system without scars has a higher energy before collapse in the $N_1 = 642$ case, while the system with scars has a higher energy before collapse in the $N_2 = 1212$ case. The configurations suggest that shells preserve their original symmetry, e.g., the symmetry in the absence of pressure, until collapse. A more quantitative way to look at it is through spherical harmonic expansions [21, 32]

$$\begin{aligned} R(\theta, \phi) &= \sum_i R_i \delta(\phi - \phi_i)\, \delta(\cos\theta - \cos\theta_i) \\ &= \sum_{l,m} Q_{lm} Y_{lm}(\theta, \phi), \end{aligned} \tag{11}$$

where (R_i, θ_i, ϕ_i) represents the spherical coordinates of vertex i in the reference frame centered at the shell's center of mass. From the coefficients Q_{lm}, one may form two rotationally invariant quantities [35]

$$Q_l = \left(\frac{4\pi}{2l+1} \sum_{m=-l}^{l} |Q_{lm}|^2 \right)^{1/2} \tag{12}$$

and

$$\hat{W}_l = \frac{\sum\limits_{\substack{m_1, m_2, m_3 \\ m_1+m_2+m_3=0}} \begin{pmatrix} l & l & l \\ m_1 & m_2 & m_3 \end{pmatrix} Q_{lm_1} Q_{lm_2} Q_{lm_3}}{\left(\sum\limits_m |Q_{lm}|^2 \right)^{3/2}}. \tag{13}$$

The coefficients $\begin{pmatrix} l & l & l \\ m_1 & m_2 & m_3 \end{pmatrix}$ are Wigner $3j$ symbols [36]. For a shape with the icosahedral symmetry, the $\{Q_l\}$ are nonzero only for $l = 0,\ 6,\ 10,\ \ldots$ [35]. The magnitudes of $\{Q_l\}$ change with shape. The $\{\hat{W}_l\}$ are normalized so that they are independent of the overall magnitude of the $\{Q_{lm}\}$ for a given l. The parameters $|\hat{W}_l|$ are a direct index of the symmetry of a shape (see Ref. [35] and references therein). In Fig. 4 we plot Q_l/Q_0

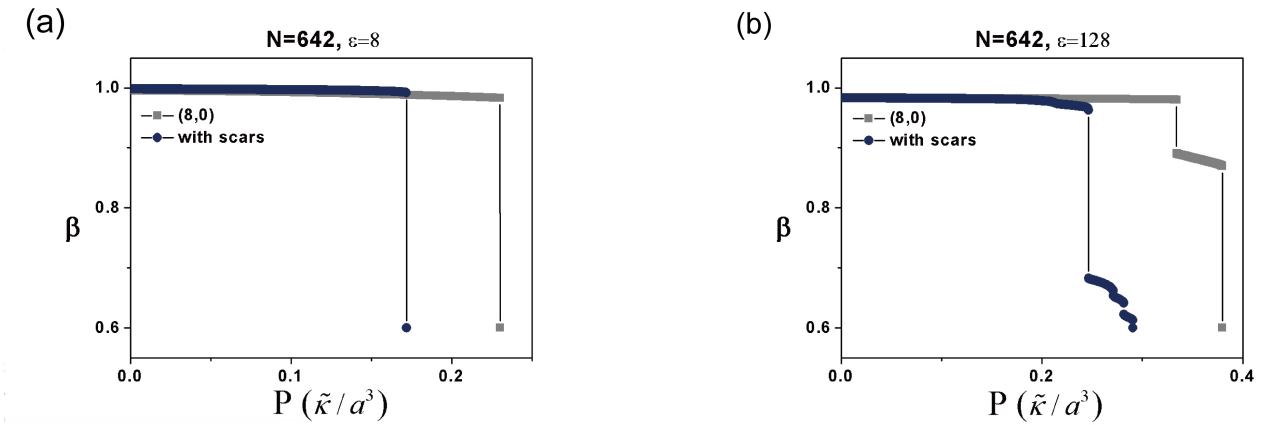

FIG. 2. (Color online) Evolution of the parameter β under the external pressure. (a) For small values of ε, shells collapse directly to β_{min}. (b) For large ε, shells collapse in stages. In the latter case, the critical pressure is defined as the point of the first collapse.

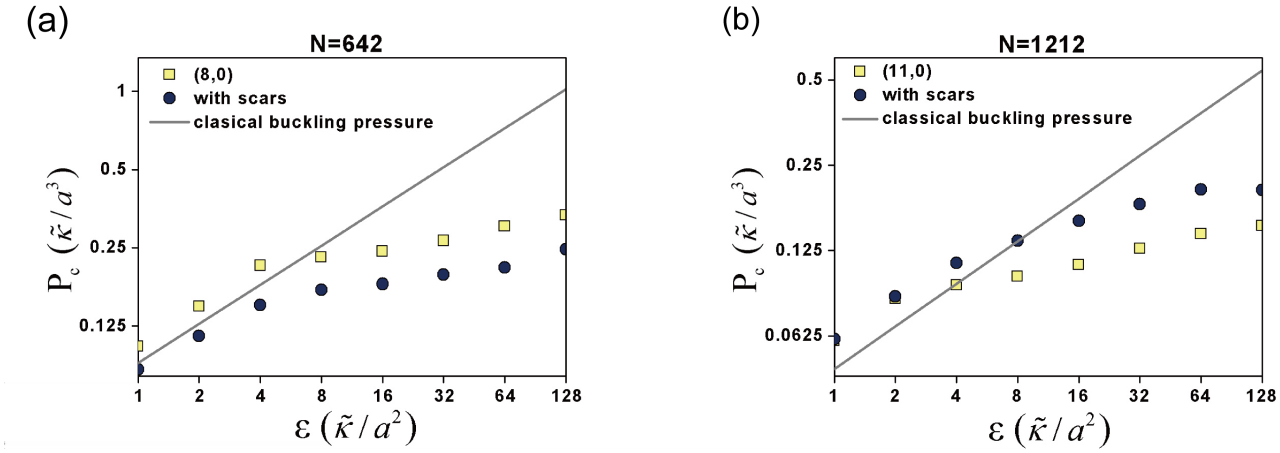

FIG. 3. (Color online) Critical pressure P_c for the $N_1 = 642$ shells (a) and the $N_2 = 1212$ shells (b). The grey lines indicate the buckling pressure of ideal spherical shells as predicted by continuum elastic theory.

and in Table I we compare $|\hat{W}_l|$ with the characteristic values for an icosahedral symmetry given in Ref. [35]. Except for small errors that are likely to be due to numerical accuracy, the results agree well with previous findings. In the $N_2 = 1212$ case, both shells preserve icosahedral symmetry before collapse; scars round the cones formed by disclinations and shells look less buckled compared to shells without scars, which is a reduction of the effective radius and thus leads to a higher critical pressure. Note that if we keep the area of scars fixed while increasing the radius, in the limit $R \to \infty$, we expect that the critical pressures in both cases will become indistinguishable as the effective radius reduction becomes infinitely small in this limit.

Therefore, we argue that two mechanisms affect the critical pressure: i) the preservation of icosahedral symmetry and ii) the relative area occupied by scars. As a further check, we break the icosahedral symmetry of configurations with scars by flipping a bond of one of the twelve star-like scars, in two ways shown in Fig. 5(b) and (c), and find the critical pressures are lowered significantly in both situations. We test shells with a (p, q) structure and with the total number of vertices in the 400 to 2000 range (see Appendix for details) and find results that align well with expectations.

TABLE I. $|\hat{W}_l|$ for icosahedron and shapes in Fig 4.

	$\lvert\hat{W}_6\rvert$	$\lvert\hat{W}_{10}\rvert$
Icosahedron	0.169754	0.093967
(8,0)	0.169751	0.093951
N=642,with scars	0.117793	0.002383
(11,0)	0.169751	0.093964
N=1212,with scars	0.169751	0.093968

During the collapse, we find emergence of configurations with a broken icosahedral symmetry. Fig. 6 shows configurations at $\beta = 0.8$. With ε increasing, the shell

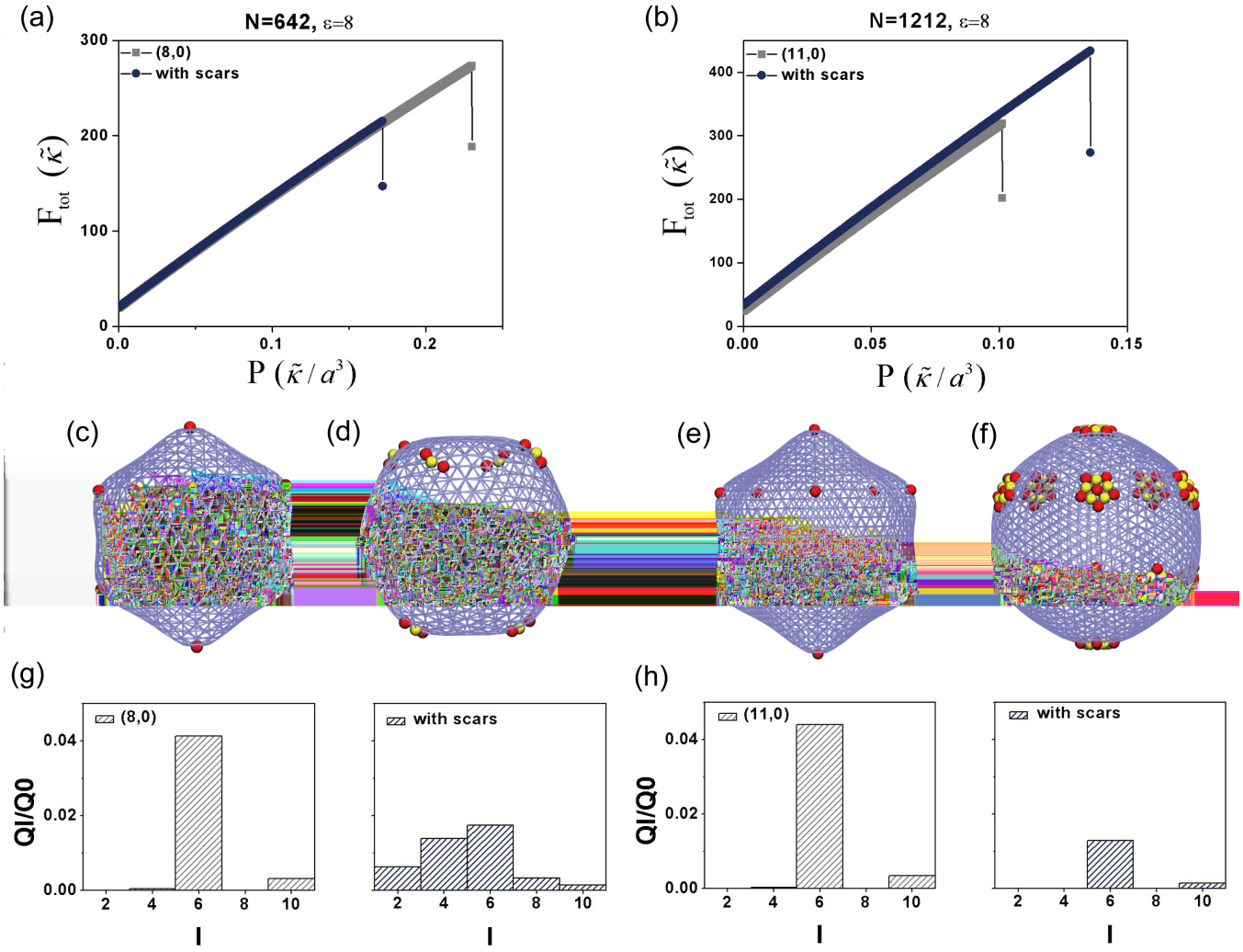

FIG. 4. (Color online) Plots of the evolution of the system energy F_{tot} for $N_1 = 642$ shells with $\varepsilon = 8$ (a) and $N_2 = 1212$ shells with $\varepsilon = 8$ (b). (c)-(f) Corresponding configurations for shells before collapse. (g)-(h) Histograms of Ql/Q0 for the configurations.

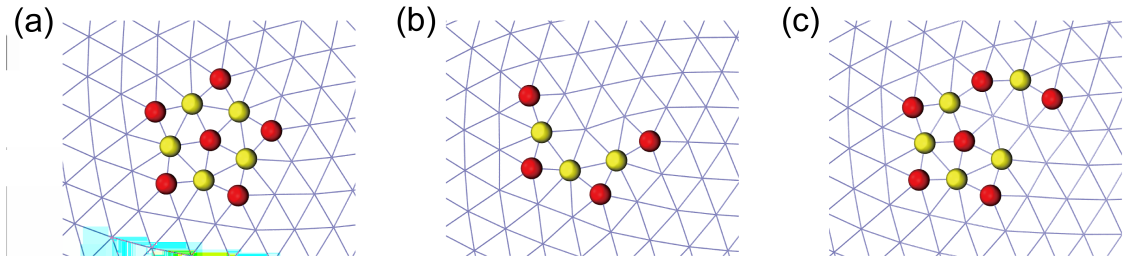

FIG. 5. (Color online) (a) One of the twelve star-like scars. (b)-(c) Two ways of breaking the icosahedral symmetry by flipping a bond.

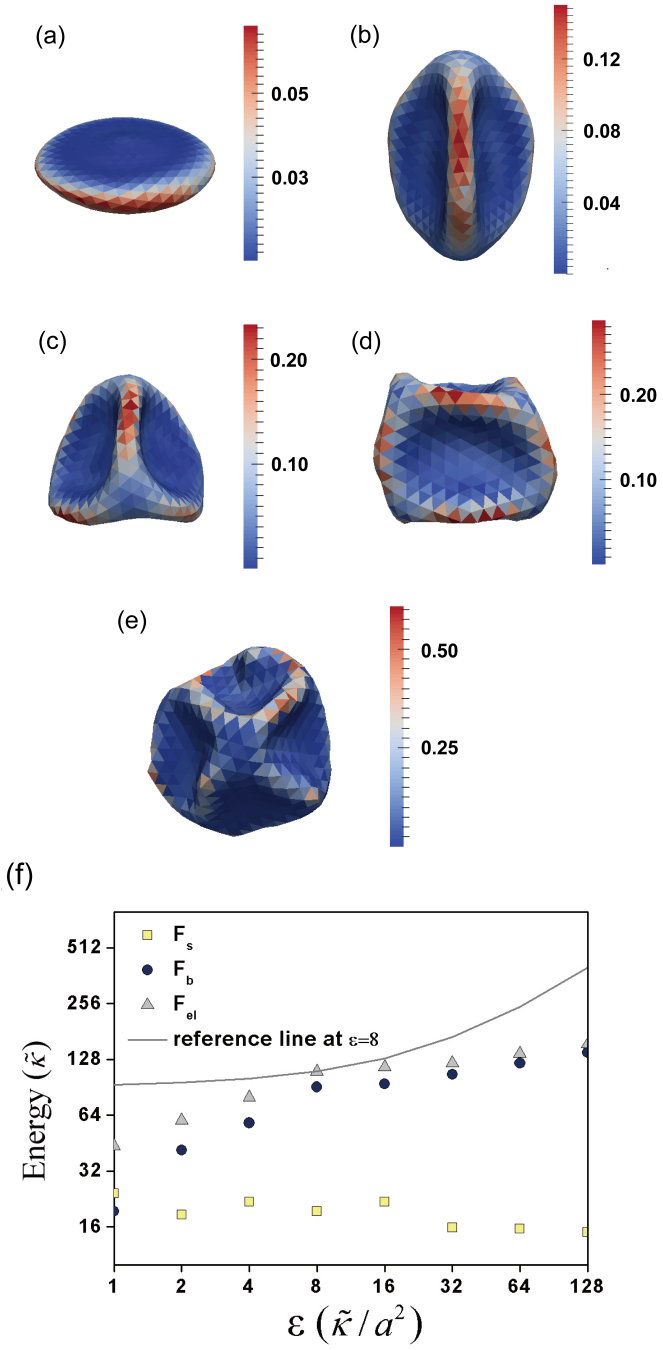

FIG. 6. (Color online) (a)-(e) Configurations of $(8,0)$ shells at $\beta = 0.8$ during collapsing, with $\varepsilon = 1, 2, 4, 8, 128$, respectively. Color represents local bending energy. (f) Energies plotted vs ε. The reference line at $\varepsilon = 8$ shows the elastic energy keeping the configuration at $\varepsilon = 8$ frozen while varying ε.

at first appears to retain a regular shape, e.g., a disk, a three-fold deflated American football, a concave tetrahedron or a squashed cube. The appearance of these shapes is not surprising since the icosahedral symmetry contains six 5-fold axes, ten 3-fold axes and fifteen 2-fold axes. In addition, an icosahedron can be decomposed into three orthogonal rectangular planes [35]. As ε increases further, irregular shapes with more ridges start to appear. These account for most of the bending energy but help to lower the overall stretching energy. A Landau-like theory of phase transitions has been constructed for the emergence of a cubic-like shape during the collapse of an icosahedral shell [32]. In the energy plot Fig. 6(f), the reference line at $\varepsilon = 8$ lies above the elastic energy at other ε values. Except for small fluctuations, we find the situation is similar for references lines at other values of ε, which indicates the configuration at a certain ε is favored compared with other configurations.

TABLE II. Symmetries of the corresponding scarred shells.

N	(p,q)	point group	N	(p,q)	point group
432	$(6,1)$	D_3	1242	$(10,2)$	C_1
482	$(4,4)$	C_2	1272	$(7,6)$	T
492	$(5,3)$	C_2	1292	$(8,5)$	$=$
492	$(7,0)$	C_2	1332	$(9,4)$	I
522	$(6,2)$	C_2	1332	$(11,1)$	I
572	$(7,1)$	D_3	1392	$(10,3)$	C_1
612	$(5,4)$	C_2	1442	$(12,0)$	C_1
632	$(6,3)$	D_3	1472	$(11,2)$	C_2
642	$(8,0)$	C_2	1472	$(7,7)$	C_2
672	$(7,2)$	C_1	1482	$(8,6)$	T
732	$(8,1)$	T	1512	$(9,5)$	I
752	$(5,5)$	C_2	1562	$(10,4)$	$=$
762	$(6,4)$	C_2	1572	$(12,1)$	I
792	$(7,3)$	T	1632	$(11,3)$	I
812	$(9,0)$	C_2	1692	$(8,7)$	I
842	$(8,2)$	C_1	1692	$(13,0)$	I
912	$(6,5)$	C_1	1712	$(9,6)$	$=$
912	$(9,1)$	C_1	1722	$(12,2)$	$=$
932	$(7,4)$	C_1	1752	$(10,5)$	I
972	$(8,3)$	T_h	1812	$(11,4)$	$=$
1002	$(10,0)$	T	1832	$(13,1)$	I
1032	$(9,2)$	C_1	1892	$(12,3)$	$=$
1082	$(6,6)$	D_5	1922	$(8,8)$	$=$
1092	$(7,5)$	T	1932	$(9,7)$	I
1112	$(10,1)$	C_1	1962	$(10,6)$	$=$
1122	$(8,4)$	C_1	1962	$(14,0)$	$=$
1172	$(9,3)$	C_1	1992	$(13,2)$	$=$
1212	$(11,0)$	I			

V. SUMMARY AND CONCLUSIONS

We used numerical simulations to show that the topological scars present in the crystalline lattice of thin shell with spherical topology affect shell's ability to sustain external hydrostatic pressure. Furthermore, we demonstrated that the distribution of the scars within the lattice, i.e., their symmetry, non-trivially affects shells' resistance to pressure. We find that the critical pressure at which shells collapse is lowered when the scar distribution breaks the icosahedral symmetry and raised when

symmetry is preserved. We find that the isotropic pressure will not alter the symmetry of shells before collapse. The emergence of shapes with a broken icosahedral symmetry during collapse for shells starting with icosahedral symmetry is a function of $\varepsilon/\tilde{\kappa}$ (FvK number γ with fixed R), with more ridges that concentrate bending energy present to lower the stretching energy for high $\varepsilon/\tilde{\kappa}$.

This is yet another example of a problem in which the frustration caused by the incompatibility between order and underlying geometry causes very non-trivial behavior, with a rich variety of shape patterns with no flat space analogues. In this study we have concentrated on a somewhat simpler case of frozen defects and only examine response of the geometry to the external perturbation. It would be interesting, yet substantially more complicated, to explore how the defect distribution evolves as a shell deforms.

ACKNOWLEDGMENTS

DW thanks M. Xiao for constructive discussions. Numerical simulations were performed using the Syracuse University campus OrangeGrid which was supported by NSF award ACI-1341006. RS thanks EPSRC (Grant No. EP/M009599/1) for funding. This research was supported by the Soft Matter Program of Syracuse University.

Appendix A: Symmetries of various shell configurations

Table II shows the (p, q) pairs of shells without scars, with the number of vertices N in the range from 400 to 2000 and the point groups the corresponding scarred configurations belong to [37], with the connectivity matrix taken from the Thomson problem database [31]. " = " indicates the configuration with scars is the same as the configuration without scars, i.e., only twelve disclinations present. In all cases except the $(8, 3)$ case, we find that within a clear definition, the critical pressure at which shells collapse is lowered for scars that break icosahedral symmetry and raised for scars that preserve icosahedral symmetry. In the $(8, 3)$ case, shells with scars have a higher critical pressure for certain ε range, we think this is partly due to T_h being a high order symmetry and partly due to it having a relatively large scar area.

[1] D. M. Knipe, P. M. Howley, *et al.*, *Fields Virology*, 6th ed. (Lippincott Williams and Wilkins, Philadelphia, PA, 2013).
[2] H. Huang, E. E. Remsen, T. Kowalewski, and K. L. Wooley, J. Am. Chem. Soc. **121**, 3805 (1999).
[3] E. Katifori, S. Alben, E. Cerda, D. R. Nelson, and J. Dumais, Proc. Natl. Acad. Sci. **107**, 7635 (2010).
[4] E. Couturier, J. Dumais, E. Cerda, and E. Katifori, Soft Matter **9**, 8359 (2013).
[5] B. Audoly and Y. Pomeau, *Elasticity and Geometry* (Oxford University Press, Oxford, 2010).
[6] A. M. A. van der Heijden, *W. T. Koiter's Elastic Stability of Solids and Structures* (Cambridge University Press, Cambridge, 2009).
[7] L. Landau and E. Lifshitz, *Theory of Elasticity*, 3rd ed. (Butterworth-Heinemann, Singapore, 1999).
[8] A. V. Pogorelov, *Bendings of Surfaces and Stability of Shells*, Vol. 72 (American Mathematical Society, Providence, RI, 1988).
[9] J. Paulose, G. A. Vliegenthart, G. Gompper, and D. R. Nelson, Proc. Natl. Acad. Sci. **109**, 19551 (2012).
[10] M. P. D. Carmo, *Differential Geometry of Curves and Surfaces* (Prentice-Hall, Inc., Upper Saddle River, NJ, 1976).
[11] S. Sachdev and D. R. Nelson, J. Phys. C **17**, 5473 (1984).
[12] D. Caspar and A. Klug, Cold Spring Harb. Symp. Quant. Biol. **27**, 1 (1962).
[13] M. J. Bowick, D. R. Nelson, and A. Travesset, Phys. Rev. B **62**, 8738 (2000).
[14] M. Bowick, A. Cacciuto, D. R. Nelson, and A. Travesset, Phys. Rev. Lett **89**, 185502 (2002).
[15] A. Pérez-Garrido, M. J. W. Dodgson, and M. A. Moore, Phys. Rev. B **56**, 3640 (1997).
[16] J. J. Thomson, Phil. Mag **7**, 237 (1904).
[17] A. R. Bausch, M. J. Bowick, A. Cacciuto, A. D. Dinsmore, M. F. Hsu, D. R. Nelson, M. G. Nikolaides, A. Travesset, and D. A. Weitz, Science **299**, 1716 (2003).
[18] T. Einert, P. Lipowsky, J. Schilling, M. J. Bowick, and A. R. Bausch, Langmuir **21**, 12076 (2005).
[19] M. J. Bowick, L. Giomi, H. Shin, and C. K. Thomas, Phys. Rev. E **77**, 021602 (2008).
[20] H. S. Seung and D. R. Nelson, Phys. Rev. A **38**, 1005 (1988).
[21] J. Lidmar, L. Mirny, and D. R. Nelson, Phys. Rev. E **68**, 051910 (2003).
[22] A. Šiber and R. Podgornik, Phys. Rev. E **79**, 011919 (2009).
[23] C. M. Funkhouser, R. Sknepnek, and M. O. de la Cruz, Soft Matter **9**, 60 (2013).
[24] A. Šiber, Phys. Rev. E **73**, 061915 (2006).
[25] C. Q. Ru, J. Appl. Phys. **105**, 124701 (2009).
[26] N. K. Varde and D. W. Pack, Expert Opin. Biol. Ther. **4**, 35 (2004).
[27] G. A. Vliegenthart and G. Gompper, New J. Phys. **13**, 045020 (2011).
[28] J. Paulose and D. R. Nelson, Soft Matter **9**, 8227 (2013).
[29] B. A. Dubrovin, A. T. Fomenko, and S. P. Novikov, *Modern Geometry*, Vol. 1 (Springer, New York, 1984).
[30] B. Schmidt and F. Fraternali, J. Mech. Phys. Solids **60**, 172 (2012).
[31] C. Cecka, M. Bowick, A. Middleton, L. Giomi, and K. Zielnicki, "Thomson problem @ S.U." `http://thomson.phy.syr.edu/thomsonapplet.php`.

[32] E. H. Yong, D. R. Nelson, and L. Mahadevan, Phys. Rev. Lett **111**, 177801 (2013).
[33] W. Humphrey, A. Dalke, and K. Schulten, J. Mol. Graphics **14**, 33 (1996).
[34] J. Stone, Master's thesis, Computer Science Department, University of Missouri-Rolla (1998).
[35] P. J. Steinhardt, D. R. Nelson, and M. Ronchetti, Phys. Rev. B **28**, 784 (1983).
[36] L. D. Landau and L. M. Lifshitz, *Quantum Mechanics*, 3rd ed. (Butterworth-Heinemann, Oxford, 1977).
[37] D. J. Wales and S. Ulker, Phys. Rev. B **74**, 212101 (2006).